



Numerical Study of Reverse Thrust Generation Using Co-Flow Jet

Daniel Perlin[†], GeCheng Zha[‡]
Dept. of Mechanical and Aerospace Engineering
University of Miami, Coral Gables, FL 33146
Email: gzha@miami.edu

Abstract

This paper studies a new reversed thrust generation method for airfoils by use of active flow control altered from the regular Co-Flow Jet (CFJ) airfoil. This reverse thrust is generated by a CFJ injection slot duct that is redirected to flow against the freestream flow direction, rather than injecting flow tangentially to the main flow behind the leading edge. Such an injection jet can disrupt the flow with considerable flow separation, thereby decreasing the lift coefficient (C_l) and increasing the drag coefficient (C_d). Three configurations of the reverse thrust CFJ concept are derived from a CFJ-NACA 6421 CFJ airfoil to compare the performance characteristics and determine the most effective approach to achieving maximal C_d and minimal C_l with low energy expenditure. The three configurations studied include an injection slot directed upward, an injection slot directed directly outward against the freestream, and an injection slot directed downward. The regular CFJ airfoil and the baseline airfoil with no flow control are also simulated for comparison. All three configurations are simulated, along with a regular CFJ airfoil, at a jet momentum coefficient (C_{μ}) of 0.03, 0.1, 0.2, 0.3, and 0.4, at angles of attack between 0° and 70° , and at a Mach number $M = 0.15$. The results for the CFJ configurations are compared with the baseline NACA 6421 airfoil. It reveals the forward-facing injection to be the most effective configuration in general, particularly at high AoA, between 15° and 60° , and $C_{\mu} = 0.2 \sim 0.3$, with inverse aerodynamic efficiencies C_d/C_l increased by up to 993% compared with the baseline NACA 6421 airfoil. The forward injection also requires substantially lower CFJ power than the downward and upward injection. At low angles of attack, AoA = $0^\circ \sim 10^\circ$, downward injection appears to be more effective, using $C_{\mu} = 0.2 \sim 0.3$, with C_d/C_l increased by 330% to 480% compared with the baseline airfoil C_d/C_l .

[†]: Recent Undergraduate Student

[‡]: Professor

Nomenclature

AoA	Angle of attack
CFD	Computational Fluid Dynamic(s)
CFJ	Co-Flow Jet
ESTOL	Extremely short takeoff and landing
VTOL	Vertical takeoff and landing
FASIP	Flow-Acoustics-Structure Interaction Package
C_l	Lift coefficient
C_d	Drag coefficient
C_m	Moment coefficient
C_μ	Jet momentum coefficient; $\dot{m}_j U_j / (q_\infty S)$
$C_{l_{max}}$	Maximum lift coefficient at a constant C_μ
C_d/C_l	Inverse aerodynamic efficiency; $1/(C_l/C_d)$
P_c	Power coefficient; $L / (q_\infty S V_\infty)$
P_r	Pressure ratio; P_{ti}/P_{ts}
P_{ti}	Total injection pressure
P_{ts}	Total suction pressure
M	Mach number
\dot{m}	Mass flow
U	Flow velocity
q_∞	Freestream dynamic pressure
S	Planform area (unit planform area for 2D)
V_∞	Freestream velocity
α	Angle of attack
c	Subscript, stands for corrected
j	Subscript, stands for jet

1. Introduction

1.1. Background

Traditionally, airplanes have relied on three primary means of braking after landing: flaps, spoilers, and engine thrust reversers. Both flaps and spoilers simply modify the profile of a wing's airfoil shape, acting as passive braking methods, in order to change the aerodynamic characteristics of the wing while remaining in a fixed position. The use of active reverse thrust from engines, typically found on larger aircraft, relies on applying work on an enclosed region of air in order to augment braking capability. There are various techniques which aircraft currently employ to incorporate reverse thrust.

While piston-engine prop aircraft typically do not have reverse thrust capabilities, variable-pitch turboprop airplanes frequently have reversible propellers. A reversible propeller is achieved simply by rotating the propeller blade to a negative pitch, opposite from the typical pitch angle direction with respect to the ground idle position, as demonstrated in the figure below.

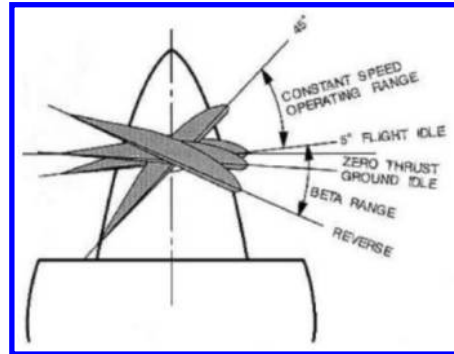


Figure 1: Variable-pitch propeller with reverse thrust, plot adopted from [1]

Jet engines employ a wider variety of reverse thrust methods. However, while there are several variations, these thrust reversers can generally fit into three common categories. The bucket thrust reverser, known also as the target thrust reverser, involves rotating and translating two panels of the outer fairing of the jet engine with a mechanical linkage system to block and redirect the exiting exhaust flow as shown in Figure 2. An alternative system used both in turbojet and turbofan engines is the clamshell door or pivoting door thrust reverser, which behaves similarly, but integrates the panels further upstream within the jet engine, blocking the flow before the exhaust or bypass air reaches the nozzle. Finally, turbofan engines, usually receiving the majority of their thrust from bypass air, can also employ cold-stream reversers, also known as cascade reversers, which block only the cooler bypass air, rather than hot jet exhaust, redirecting this flow through angled “cascade” fins. (See Figure 2 below)

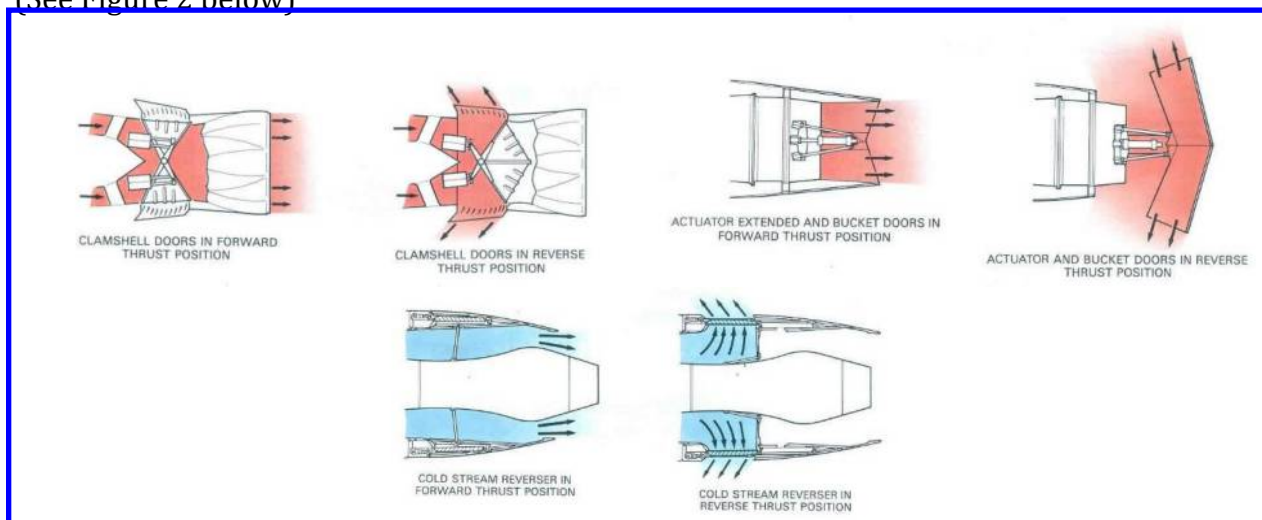


Figure 2: Thrust reversers found on jet engines, including clamshell door reversers (top left), bucket reverser (top right), and cold-stream reverser (bottom), plot adopted from [2]

1.2. Objective

The objective of this study is to simulate and analyze a new form of in-wing active flow control to induce reverse thrust, by using a modified Co-Flow Jet (CFJ) airfoil. This design concept holds its motivation in driving forward advancements in the field of active flow control, particularly for purposes such as the elimination of control surfaces, emphasized in [3]. Hence, this may be an effective supplement or alternative to thrust reversers in conventional aircraft. It may also support the reduction or even removal of the need for spoilers or other control surfaces on aircraft equipped with CFJ wings, helping to potentially reduce both cost and weight due to the hydraulic system. In this paper, three potential configurations of the reverse thrust CFJ airfoils are studied in a 2D steady-state CFD model at varying AoA and C_{μ} .

1.3. Co-Flow Jet

Co-Flow Jet is a zero-net-mass-flux active flow control concept recently developed by Zha et al., which provides very high lift and low drag on airfoils and wings, while using low power consumption [4, 5, 6, 7, 8, 9, 10]. As a result of the exceptionally high $C_{l_{max}}$ possible with a CFJ, the lower stall velocity can allow for decreased landing and takeoff distances. Flight range can also be improved due to the aforementioned increase in lift coefficient and decrease in drag coefficient with low power consumption, and at high C_{μ} an aircraft can even perform extremely short takeoff and landing (ESTOL) [8, 9, 11, 12, 13].

Figure 3 illustrates a baseline airfoil and the equivalent CFJ airfoil, while the model in Figure 4 depicts one example of CFJ implementation into a wing segment. As shown in Figure 3, a CFJ wing consists of an energized jet of air which is created by placing a series of compressors along the wingspan, sucking in air along the suction surface near the trailing edge of the wing, feeding the air through the compressors, and injecting the air along the suction surface near the leading edge. By both energizing the boundary layer flow near the leading edge with the injection jet and creating the suction near the trailing edge of the wing, flow separation can be delayed to very high angle of attack, such as over 65° . The injection of air along the suction wall at high angle of attack reduces the peak suction pressure, allowing for much higher $C_{l_{max}}$ than a baseline airfoil. Since the injection slot is located near the region of lowest pressure on the airfoil, the power consumption is low. [10]

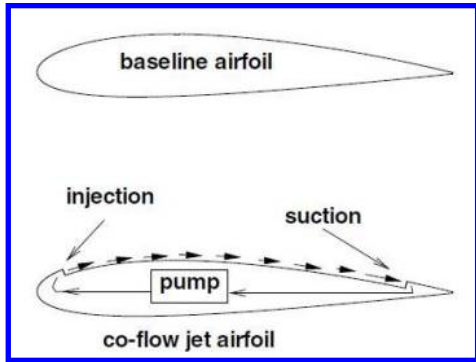


Figure 3: Baseline airfoil and Co-Flow Jet airfoil [10]

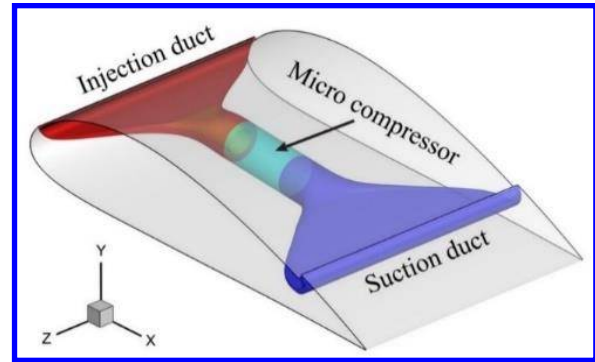


Figure 4: Model of a Co-Flow Jet wing section [4]

2. Reverse Thrust CFJ Airfoil

Since a CFJ wing inherently possesses a blowing air system provided by the imbedded compressors along the span, the blowing air mass flow can be used to disrupt the flow to increase the drag and reduce the lift, which creates the reverse thrust effect to shorten the braking distance after the aircraft touches down on the runway. This is an opposite effect that the CFJ is intended to achieve at takeoff, cruise, and landing before the aircraft touches down.

This reverse thrust airfoil concept is modified from the regular CFJ airfoil by altering the injection duct. When the injection is redirected, the original CFJ duct outlet section is closed and becomes a cavity. As shown in Figure 5, three configurations are created and studied, which vary in the flow behavior at the injection duct near the leading edge of the airfoil, directing a jet of air either directly downwards, forwards, or upwards with the objective of disrupting surrounding air flow as it passes across the airfoil. This study varies the AoA of each configuration to find if any or all configurations are effective and efficient in reducing lift while maximizing drag, observing how the outputs compare with one another against the baseline NACA 6421 airfoil and a regular CFJ in the same conditions. Due to the variability in effectiveness of CFJ based on power consumption levels, the jet momentum coefficient C_{μ} is also varied. This is conducted to see how the flow is affected to determine an optimal C_{μ} range such that significant reverse thrust capability is achieved while using a low power consumption.

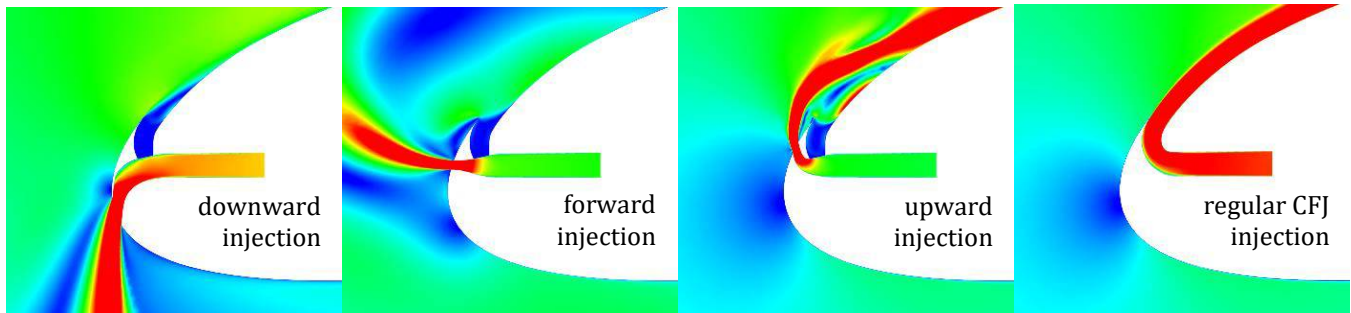


Figure 5: Reverse thrust airfoil configurations and flow fields for downward injection (far left) forward injection (2nd left), upward injection (2nd right), and regular CFJ injection (far right)

The CFD simulation and analysis conducted includes varying the AoA between 0° to 70° , in 5° increments between 0° and 30° , then 10° increments up to 70° , as well as varying the jet momentum coefficient C_μ between 0.03, 0.1, 0.2, 0.3, and 0.4. These results are all run against the baseline airfoil and regular CFJ. In total, 231 simulations are conducted. All cases use an NACA 6421 airfoil or NACA 6421 derived CFJ airfoil and are simulated at a Mach number of $M = 0.15$.

2.1. CFD Solver

The in-house FASIP (Flow-Acoustics-Structure Interaction Package) CFD code is used to conduct the numerical simulation. The 2D Reynolds Averaged Navier-Stokes (RANS) equations with one-equation Spalart-Allmaras [14] turbulence model is used. A 5th order WENO scheme for the inviscid flux [15, 16, 17, 18, 19, 20] and a 2nd order central differencing for the viscous terms [15, 19] are employed to discretize the Navier-Stokes equations. The low diffusion E-CUSP scheme used as the approximate Riemann solver suggested by Zha et al. [21] [16] is utilized with the WENO scheme to evaluate the inviscid fluxes. Implicit time marching method using Gauss-Seidel line relaxation is used to achieve a fast convergence rate [21]. The RANS solver is validated for CFJ airfoil simulations [10, 22, 23, 24, 25, 26].

2.2. Performance of Reverse Thrust CFJ Airfoil Configurations

As a result of inducing highly disruptive flow patterns while being conducted in a steady-state simulation, some of the CFD simulations for the reverse thrust configurations are difficult to converge to steady state solutions due to inherent unstable vortical flows, particularly at very high angles of attack. In two instances where $\text{AoA} = 70^\circ$, the simulation diverges, where the regular CFJ (labeled as conv. CFJ in the plots) and baseline airfoil at $\text{AoA} = 70^\circ$ manage to converge by several orders of magnitude using very similar fine mesh. Due to some of these results being unable to converge, in the interest of avoiding poor quality simulations, $\text{AoA} = 70^\circ$ cases are omitted, except for $\text{AoA} = 70^\circ$ at $C_\mu = 0.3$ for downward injection, used for interpolated results for $\text{AoA} = 60^\circ$, due to an acceptable convergence. While other sets of data are recorded, only the lift, drag, and power coefficients are analyzed, in addition to the inverse aerodynamic efficiency, C_d/C_l , as these are the dominant factors which determine the best reverse thrust configuration. Figure 6 below presents

the lift coefficients at each C_{μ} value for all four injection slot configurations and baseline NACA 6421 airfoil.

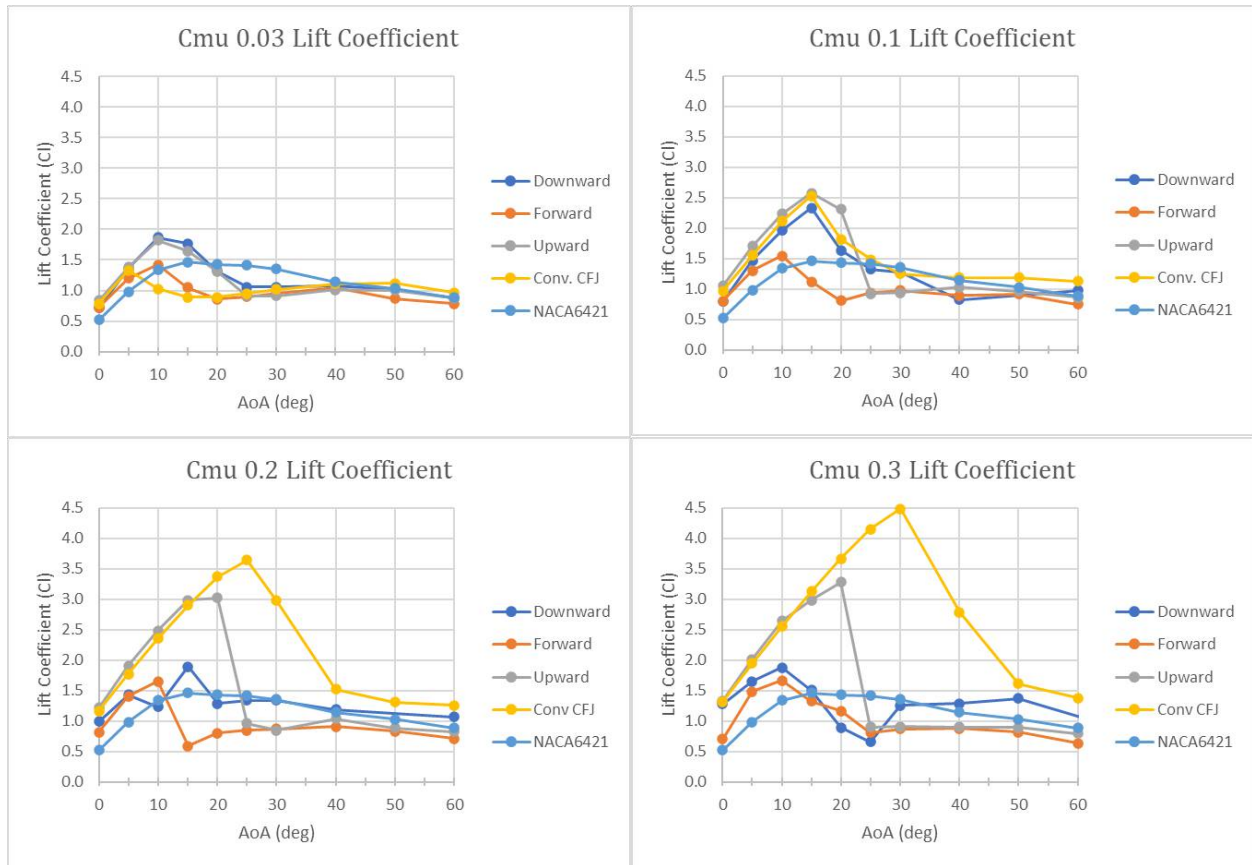


Figure 6: Lift coefficient plots at $C_{\mu} = 0.03$ (top left) $C_{\mu} = 0.1$ (top right) $C_{\mu} = 0.2$ (bottom left) and $C_{\mu} = 0.3$ (bottom right) for all 4 CFJ configurations and baseline airfoil

From the lift coefficient analysis in Figure 6 above, forward injection exhibits the lowest lift coefficient across the widest range of AoA at $C_{\mu} = 0.2 \sim 0.3$. Interestingly, for $C_{\mu} = 0.03 \sim 0.1$, the lowest lift varies between different configurations, across various AoA, even including the baseline airfoil and regular CFJ. For $C_{\mu} = 0.2$, the baseline airfoil has the lowest coefficient of lift at AoA = $0^{\circ} \sim 5^{\circ}$, with the downward injection C_l slightly lower for AoA = 10° , followed by forward injection marginally having the lowest C_l for AoA = $15^{\circ} \sim 60^{\circ}$, with one very narrow exception at AoA = 30° , where upward injection is slightly lower by less than 0.03. At AoA = 15° and $C_{\mu} = 0.2$ with forward injection, the lift is reduced by 60% compared with the baseline NACA 6421 airfoil with no flow control. For $C_{\mu} = 0.3$, the overall C_l plots, particularly at the low AoA, closely resemble $C_{\mu} = 0.2$, with the baseline holding the lowest C_l for AoA = $0^{\circ} \sim 10^{\circ}$, downward holding the lowest C_l at AoA = $20^{\circ} \sim 25^{\circ}$, closely followed by forward injection, and finally forward injection at AoA = 15° and AoA = $30^{\circ} \sim 60^{\circ}$. Equally important to minimizing the lift coefficient, however, is maximizing the drag coefficient. Figure 7 below presents the drag coefficient plots for all configurations.

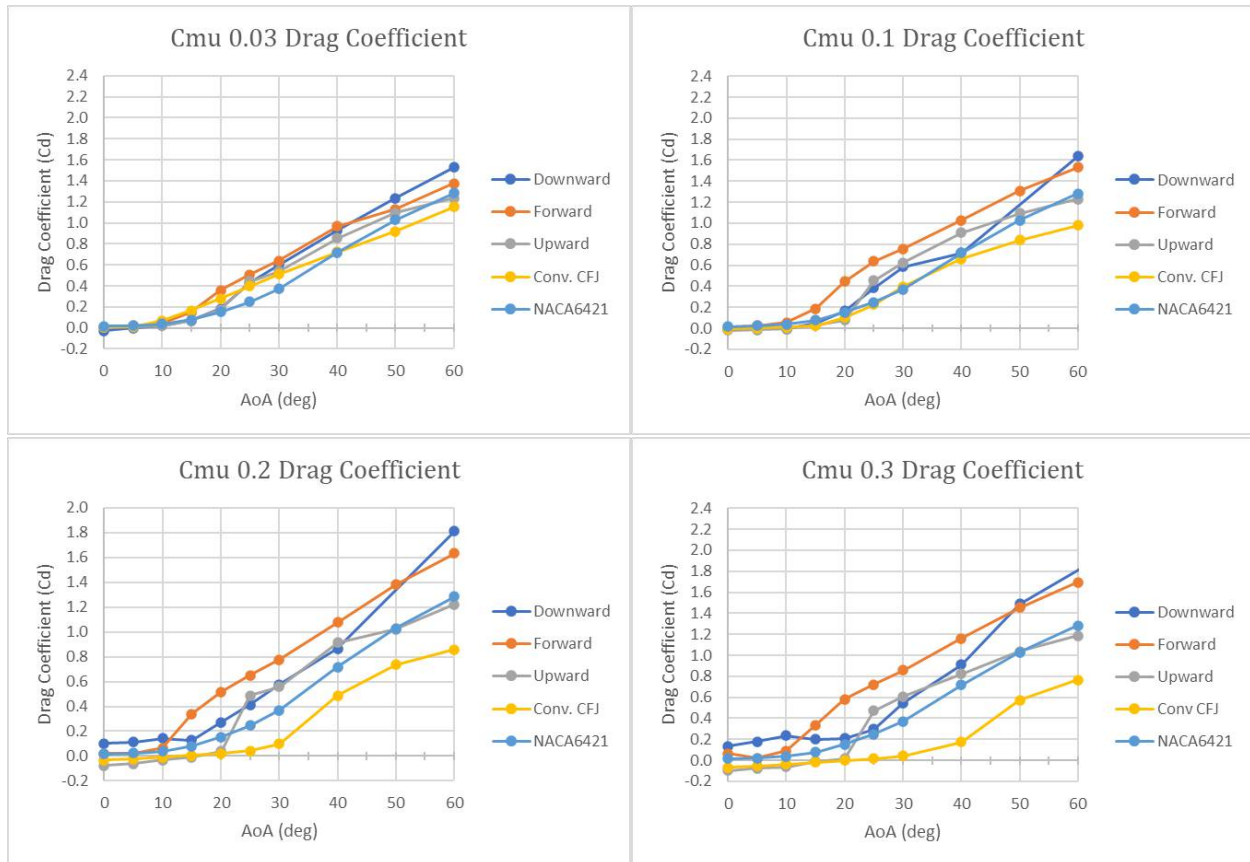


Figure 7: Drag coefficient plots at $C_{\mu} = 0.03$ (top left) $C_{\mu} = 0.1$ (top right) $C_{\mu} = 0.2$ (bottom left) and $C_{\mu} = 0.3$ (bottom right) for all 4 CFJ configurations and baseline airfoil

Under almost all circumstances, the highest drag coefficient is generated either by downward or forward injection, with forward injection tending to have the highest overall C_d for $\text{AoA} = 15^{\circ} \sim 40^{\circ}$. Notably, downward injection has drag coefficient values of around $0.1 \sim 0.2$ for $C_{\mu} = 0.2 \sim 0.3$ and $\text{AoA} = 0^{\circ} \sim 10^{\circ}$, where all other configurations remain around 0.0. Unfortunately, the plots above make it hard to evaluate C_d at low AoA. By narrowing the observed AoA range to $\text{AoA} = 0^{\circ} \sim 15^{\circ}$, a tighter zoom can be made on the smaller drag coefficients, which are displayed in Figure 8 below, noting that the C_d ranges are not the same between the $C_{\mu} = 0.03 \sim 0.1$ plots and the $C_{\mu} = 0.2 \sim 0.3$ plots.

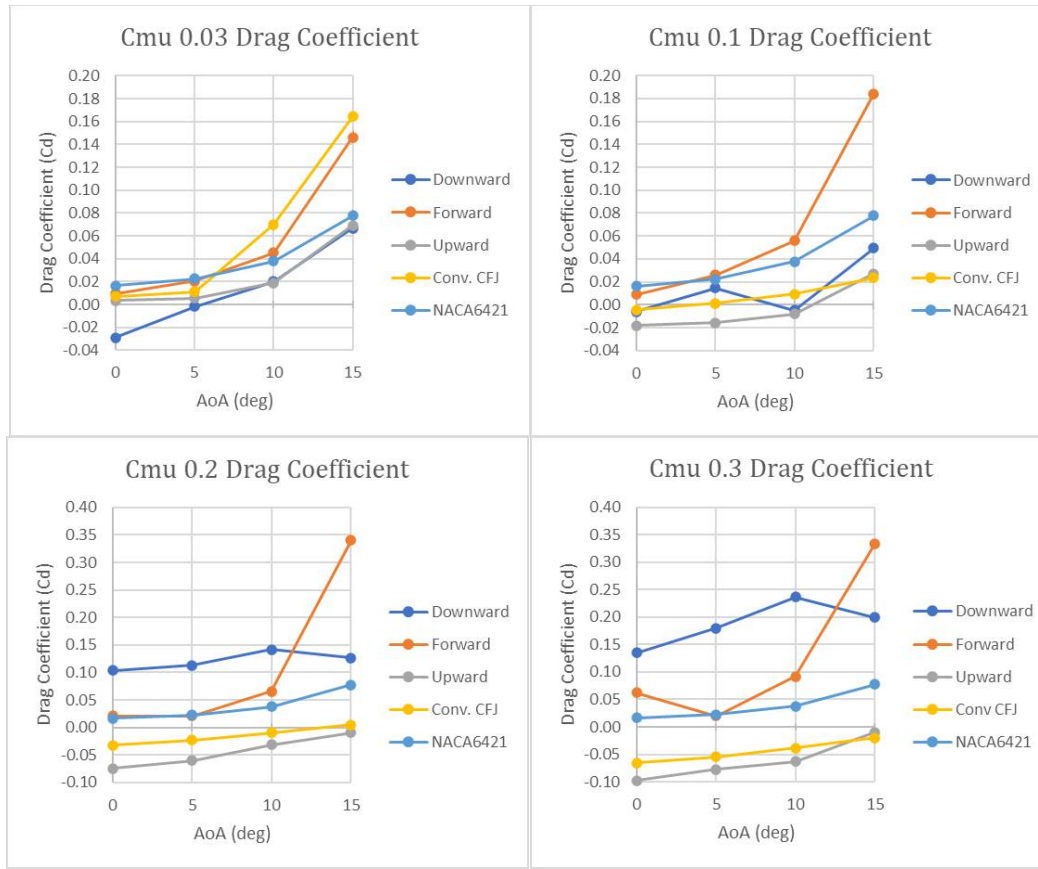


Figure 8: Drag coefficient plots at $C_{\mu} = 0.03$ (top left) $C_{\mu} = 0.1$ (top right) $C_{\mu} = 0.2$ (bottom left) and $C_{\mu} = 0.3$ (bottom right) for all 4 CFJ configurations and baseline airfoil, at AoA = 0° ~ 15°

While in Figure 7 there is a clear trend with forward injection tending to have the highest C_d , and upward and regular CFJ tending to have the lowest C_d , at lower angles of attack, as seen in Figure 8, the trends are not as clear and consistent across varied C_{μ} and AoA. The upward injection creates a thrust component, which reduces the drag compared with the forward and downward injection. For $C_{\mu} = 0.03$ ~ 0.1 , there are tight margins between forward injection, regular CFJ configurations, and baseline airfoil, with the second highest C_d usually within a difference of only 0.02. In addition, at these low C_{μ} , the drag coefficient never exceeds 0.1 for AoA = 0° ~ 10° . However, downward injection not only shows the highest drag for $C_{\mu} = 0.2$ ~ 0.3 and AoA = 0° ~ 15° , but it more than doubles the drag relative to forward injection, which is always either the second highest alternative, or nearly identical to baseline airfoil drag. Depending on the exact angle of attack, a C_d between 0.1 and 0.25 can be expected for $C_{\mu} = 0.2$ ~ 0.3 and AoA = 0° ~ 15° .

Power consumption is also an important factor to determine the overall efficiency of the reverse thrust CFJ. Since the reverse thrust is typically used only for a very brief period after landing an aircraft, it may not require a significant amount of the overall energy used during a typical flight. However, smaller power consumption is still desirable to limit the size and weight of the CFJ system which is related to the power consumption. It is thus very useful to evaluate the power coefficients of each configuration. Figure 9 below compares the power coefficients between all four

configurations. Note that the power coefficient ranges on the y-axis are not the same for all four plots.

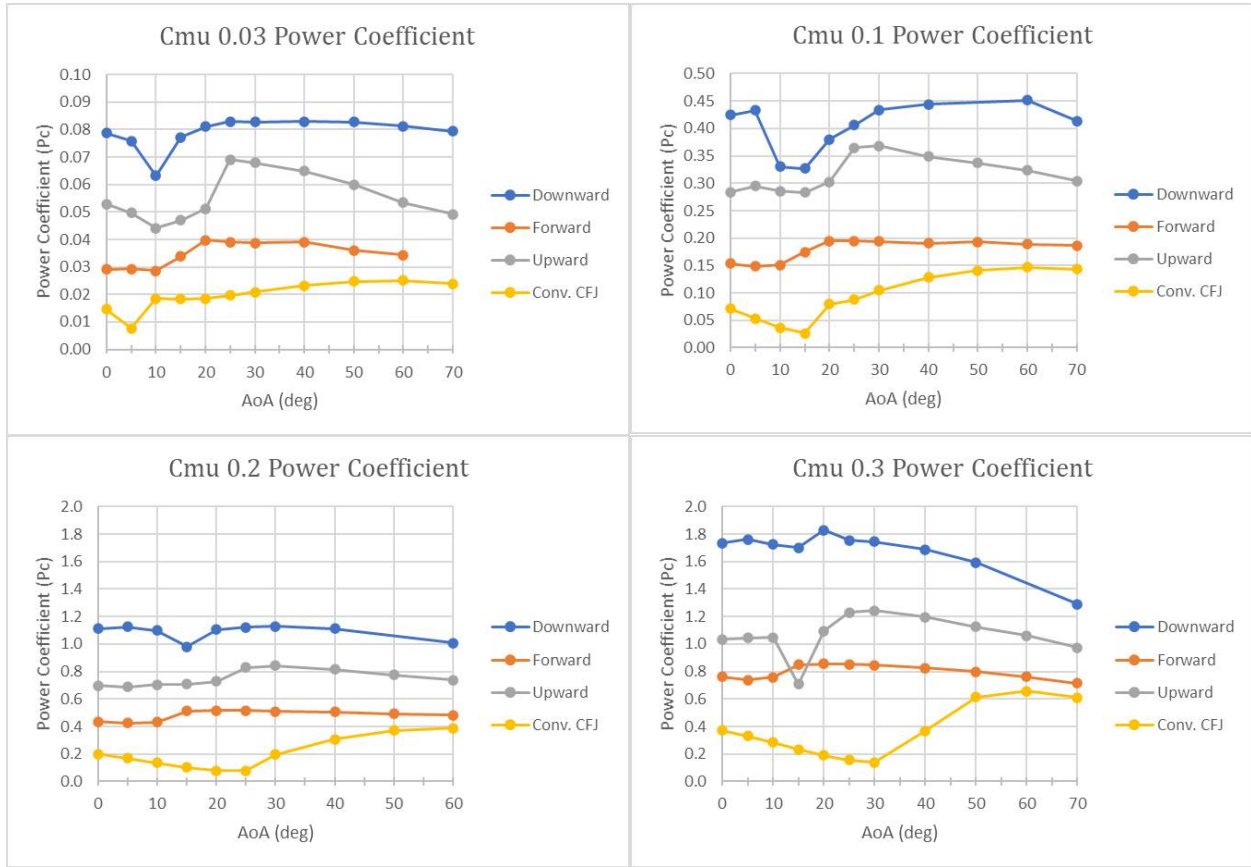


Figure 9: Power coefficient plots at $C_{\mu} = 0.03$ (top left) $C_{\mu} = 0.1$ (top right) $C_{\mu} = 0.2$ (bottom left) and $C_{\mu} = 0.3$ (bottom right) for all 4 CFJ configurations and baseline airfoil

In every C_{μ} instance above, there is a very distinct pattern showing regular CFJ with the lowest power coefficient, followed by forward injection, upward injection, and finally downward injection with the highest power coefficient. This is true in every single case, with the exception of a single data point, revealing that the power consumption for a given configuration at any state with respect to other configurations is highly predictable.

In the case of reverse thrust, the objective is to maximize drag while minimizing lift. Hence, plotting the inverse aerodynamic efficiency, C_d/C_l , acts as an effective tool to check that drag is being maximized without a proportional increase in lift. Figure 10 below shows plots of inverse aerodynamic efficiency at $C_{\mu} = 0.03$, $C_{\mu} = 0.1$, $C_{\mu} = 0.2$, and $C_{\mu} = 0.3$.

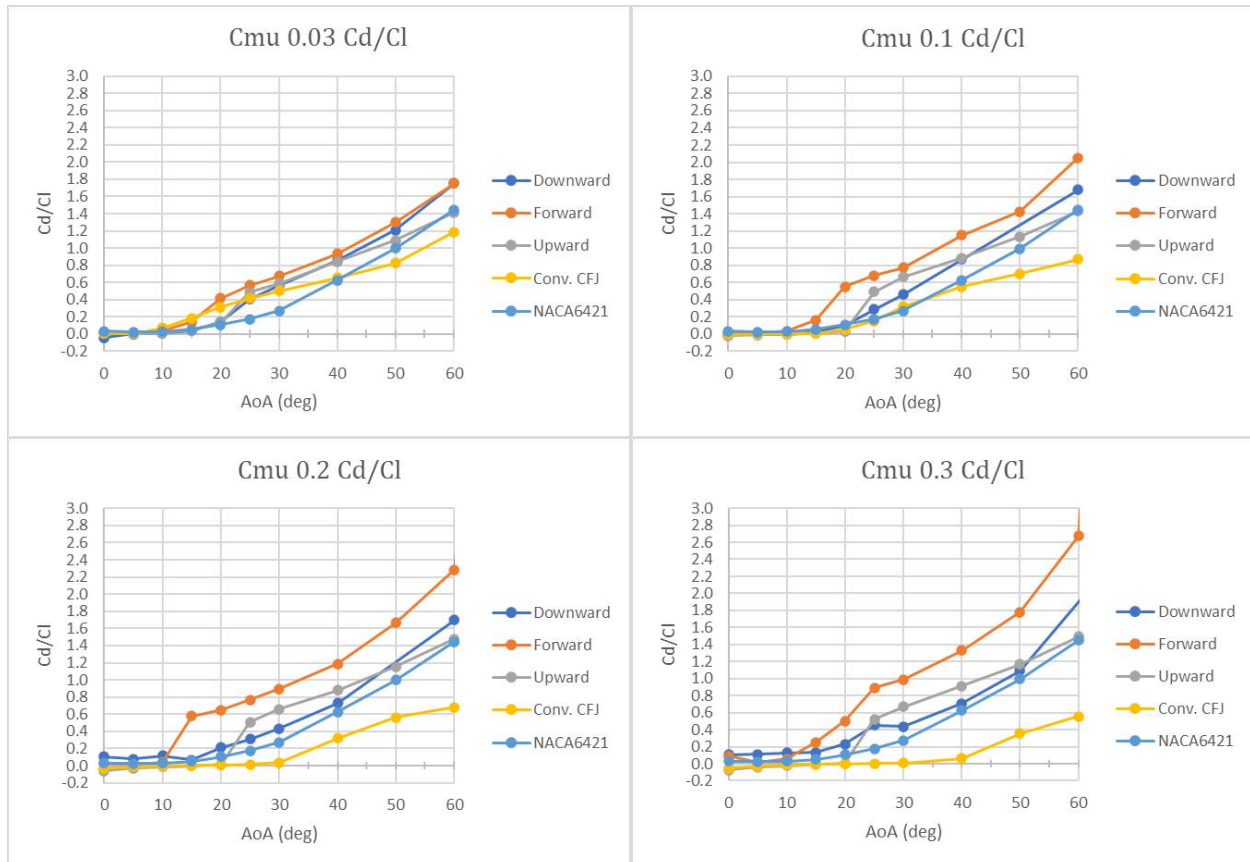


Figure 10: Inverse aerodynamic efficiency for $C_{\mu} = 0.03$ (top left) $C_{\mu} = 0.1$ (top right) $C_{\mu} = 0.2$ (bottom left) and $C_{\mu} = 0.3$ (bottom right)

While at angles of attack greater than 15° , forward injection reverse thrust consistently outperforms other configurations, at low angles of attack $AoA = 0^{\circ} \sim 10^{\circ}$, the inverse aerodynamic coefficients are very low, not exceeding 0.2. What can be discerned from the small differences for $AoA = 0^{\circ} \sim 10^{\circ}$ from Figure 10 is that, when $C_{\mu} = 0.2 \sim 0.3$, downward injection is most effective. To better compare the results, especially at lower AoA, the inverse aerodynamic efficiencies of each configuration can be viewed as a percentage change difference with respect to the baseline airfoil.

Measuring the inverse aerodynamic efficiencies with respect to the baseline simplifies direct comparison between configurations, since it allows the relative values across AoA to be standardized. By applying this standardization, it can more easily be seen that, at $C_{\mu} = 0.03$, the highest C_d/C_l varies across AoA values, with many configurations being very close in performance, whereas for $C_{\mu} = 0.1$, forward injection has the highest C_d/C_l , with a peak increase of over 400%. At $C_{\mu} = 0.2$, the peak increase is 993%. Finally, for $C_{\mu} = 0.2 \sim 0.3$, forward injection has the highest C_d/C_l for $AoA = 15^{\circ} \sim 60^{\circ}$, with downward injection outperforming for $AoA = 0^{\circ} \sim 10^{\circ}$. With the exception of $C_{\mu} = 0.03$, the regular CFJ and upward injection consistently have the lowest C_d/C_l . While the results for $C_{\mu} = 0.03$ are very “messy” compared to higher C_{μ} cases, the overall performance impact and overall effect on drag as a whole are far smaller, meaning higher C_{μ} is clearly more favorable for reverse thrust applications. (See Figure 11 below)

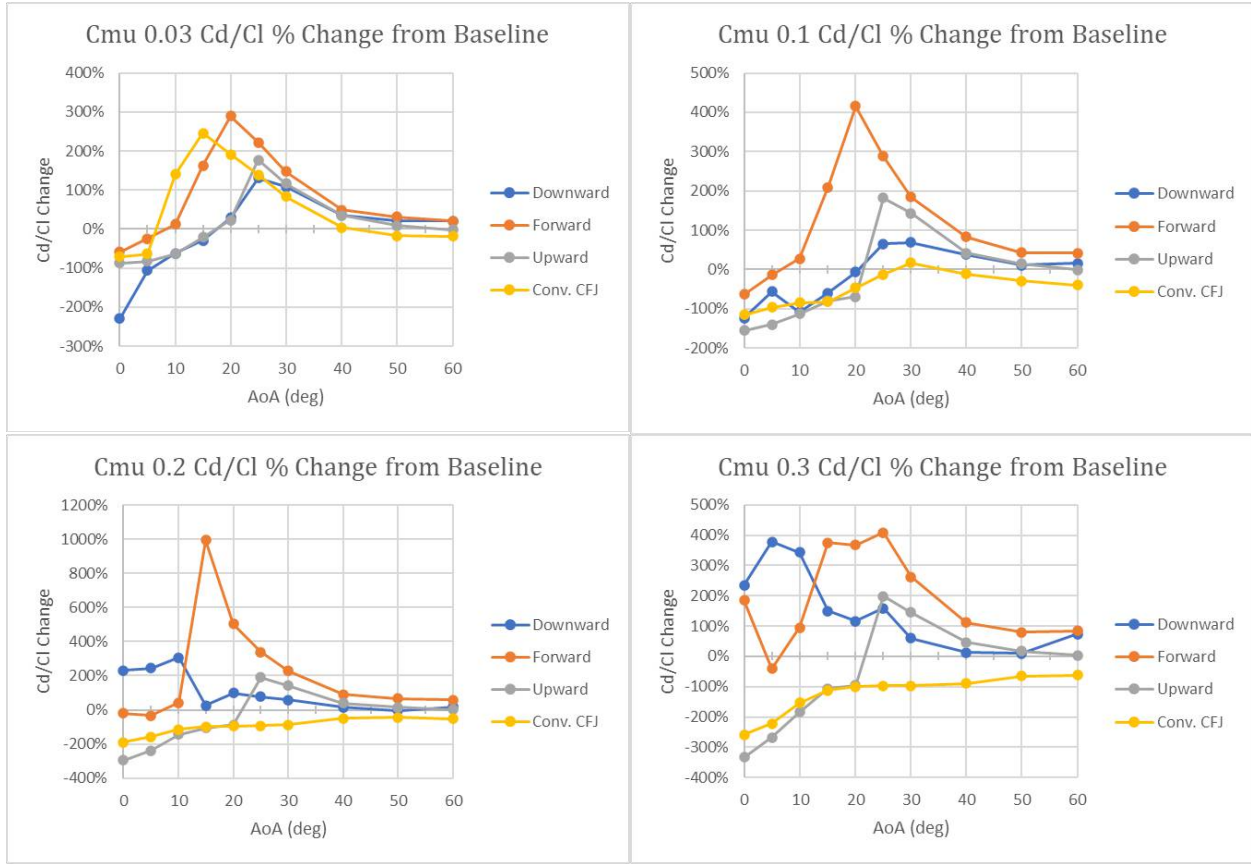


Figure 11: Percentage change in inverse aerodynamic efficiency from baseline airfoil for $C_{\mu} = 0.03$ (top left) $C_{\mu} = 0.1$ (top right) $C_{\mu} = 0.2$ (bottom left) and $C_{\mu} = 0.3$ (bottom right)

2.3. Mach Contours Comparing Reverse Thrust CFJ Airfoils

To develop a better understanding of the flow behavior, the Mach contour and streamlines across the airfoil are plotted. Among the more erratic sets of data observed above is the coefficient of lift data for the downward injection CFJ, particularly at higher C_{μ} .

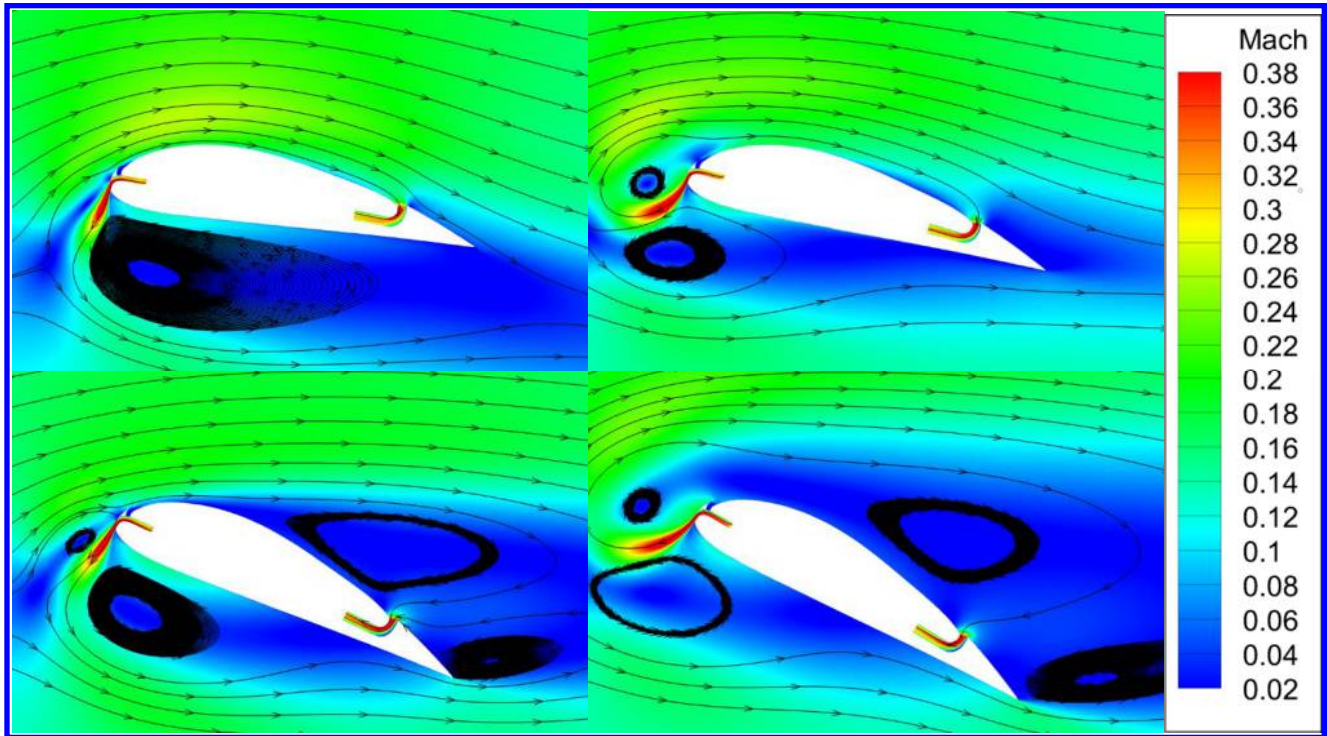


Figure 12: Mach contour plots of downward injection CFJ airfoil configuration for $C_{\mu} = 0.3$ at AoA = 10° (top left), AoA = 15° (top right), AoA = 25° (bottom left), and AoA = 30° (bottom right)

Figure 12 shows the Mach contours of the downward injection CFJ airfoil at AoA of 10° , 15° , 25° , and 30° with $C_{\mu} = 0.3$. At AoA of 10° , the downward injection creates a flow blockage and forms a large flow separation on the pressure surface of the airfoil. On the suction surface, the flow is well attached. The overall lift coefficient is substantially lower than the regular CFJ airfoil, but the peak lift coefficient is obtained at AoA = 10° . When the angle of attack is further increased, the lift coefficient decreases. The separation on the pressure surface remains but moves upstream and becomes a little smaller. At AoA = 15° , the injection jet also creates a vortex on its upper side due to the jet direction opposite to the mainstream. With the AoA continues to increase, a large separation is formed on the suction surface. The flow structures also create a large drag.

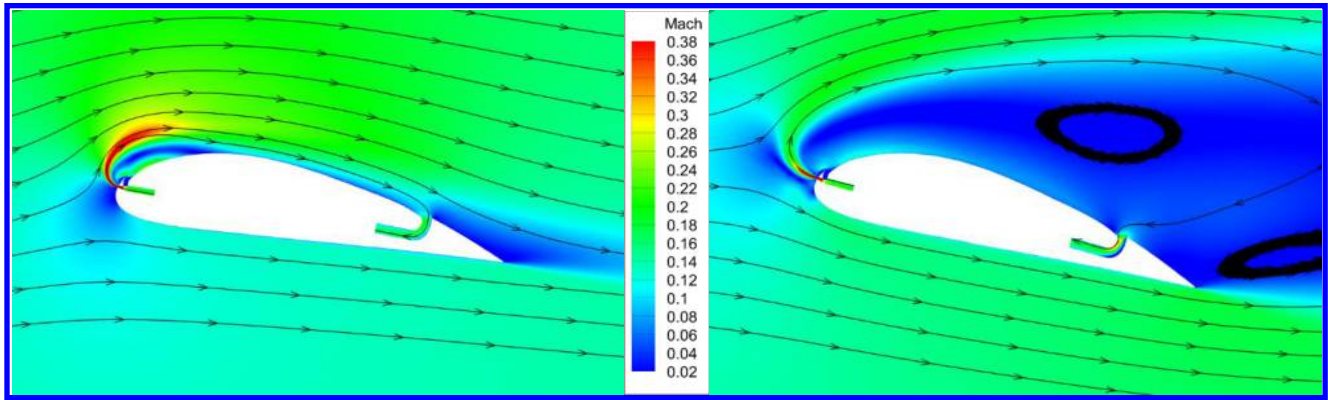


Figure 13: Forward injection CFJ airfoil Mach contour at AoA = 10° (left) and AoA = 15° (right), for $C_{\mu} = 0.2$

Among the three configurations, the forward injection appears to be the most effective to decrease the lift and increase the drag in most of the flow conditions. Figure 13 shows the flow structures at AoA = 10° and 15°. A clear difference from the downward injection is that the flow on the suction side is largely disrupted with a large separation when the AoA is 15°, which contributes to the lift reduction and drag increase. The flow on the pressure surface of the airfoil remains attached.

Figure 14 compares the Mach contour plots of the three reverse thrust CFJ airfoils with the regular CFJ airfoil at $C_{\mu} = 0.3$ with an AoA = 15°.

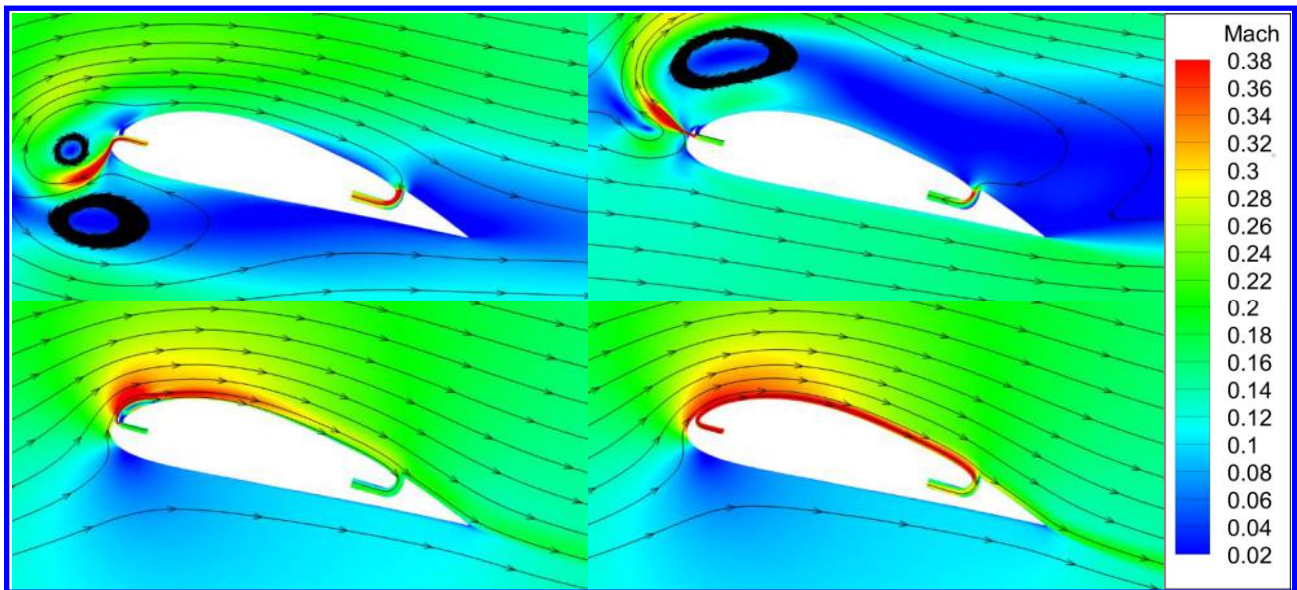


Figure 14: Downward injection (top left), forward injection (top right), upward injection (bottom left) CFJ airfoil, and regular CFJ airfoil (bottom right) Mach contour, for $C_{\mu} = 0.3$ at AoA = 15°

Clearly, the forward injection CFJ airfoil is the only one that disrupts the flow severely with a large separation on the suction surface. Downward injection has the separation mostly on the pressure surface. The least disruption is from the upward injection, which has higher drag and

lower lift than the regular CFJ airfoil, but still mostly maintains the flow attached. However as shown in Figure 6 through Figure 11, when the AoA is greater than 25° , the reverse thrust effect of the downward injection exceeds the downward injection, but still less than the forward injection and the power coefficient is also substantially higher.

3. Conclusion

This study indicates that the reverse thrust CFJ airfoil altered from a regular Co-Flow jet can be achieved with relative ease to decrease lift and increase drag, by including an additional short duct at the leading edge, and a panel that can switch between blocking either the regular CFJ injection duct or the appended thrust reverser injection duct. While this study does not focus on the aspect of the optimal design and is more on a preliminary investigation, it provides important qualitative understanding of the effectiveness. Three reverse thrust CFJ airfoils altered from the regular CFJ-NACA-6421 airfoil are simulated and compared with the regular CFJ airfoil and the baseline NACA-6421 airfoil with no flow control. The forward injection configuration proves to be highly effective in the AoA = $15^\circ\sim 60^\circ$ range with $C_\mu = 0.2\sim 0.3$, with the inverse aerodynamic efficiency C_d/C_l increased by up to 993%. The reason for this is the forward injection most severely disrupts the flow on the suction surface with a large flow separation. The downward injection creates a flow separation more on the pressure side. At low AoA, the upward injection still mostly maintains the flow attached. At low AoA, the downward injection, with $C_\mu = 0.2\sim 0.3$, appears to be the most effective to generate reverse effect for AoA = $0^\circ\sim 10^\circ$. However, when the AoA is greater than 15° , the upward injection disrupts the flow more than the downward injection. The other very appealing advantage of the forward injection is that it has the lowest CFJ power consumption across all the AoA and C_μ . The highest power consumption is from the downward injection, while the upward injection is in between. Combining all the effectiveness of the reverse thrust and power consumption, the forward injection CFJ airfoil is the most desirable option. Further study will be conducted for further optimization to understand the most sensitive design parameters.

4. Acknowledgement

All simulations are conducted on the Pegasus supercomputing system at the Center for Computational Sciences at the University of Miami.

Disclosure: The University of Miami and Dr. GeCheng Zha may receive royalties for future commercialization of the intellectual property used in this study. The University of Miami is also equity owner in Co-Flow Jet, LLC, licensee of the intellectual property used in this study.

References

- [1] I. R. McAndrew, E. Navarro and K. Witcher, "Propeller Design Requirements for Quadcopters Utilizing Variable," *International Journal of Materials, Mechanics and Manufacturing*, 6(1), 2018.
- [2] Purdue School of Aeronautics and Astronautics, "Turbine Engine Basics: Thrust Reversing," [Online]. Available: <https://engineering.purdue.edu/~propulsi/propulsion/jets/basics/reverse.html>. [Accessed 28 Nov. 2021].
- [3] Defense Advanced Research Projects Agency, "DARPA Awards Contracts for New X-Plane Program Based on Active Flow Control," 20 Sept. 2020. [Online]. Available: <https://www.darpa.mil/news-events/2020-07-20>. [Accessed 28 Nov. 2021].
- [4] K. Xu and G. Zha, "High Control Authority 3D Aircraft control Surfaces Using Co-Flow Jet," in *AIAA AVIATION Forum*, Dallas, TX, 2019.
- [5] Y. Wang and G. Zha, "Study of Mach Number Effect for 2D Co-Flow Jet Airfoil at Cruise Conditions," in *AIAA AVIATION Forum*, Dallas, TX, 2019.
- [6] G. Zha, Y. Yang, Y. Ren and B. McBreen, "Super-Lift and Thrusting Airfoil of Coflow Jet Actuated by Micro-Compressors," in *AIAA AVIATION Forum*, Atlanta, GA, 2018.
- [7] B. Wang, B. Haddoukessouni, J. Levy and G. Zha, "Numerical Investigations of Injection-Slot-Size Effect on the Performance of Coflow Jet Airfoils," *Journal of Aircraft*, Coral Gables, FL, 2008.
- [8] G. Zha, B. F. Carroll, C. D. Paxton, C. A. Conley and A. Wells, "High-Performance Airfoil Using Coflow Jet Flow Control," *AIAA Journal*, Coral Gables, FL, 2007.
- [9] G. Zha, W. Gao and C. D. Paxton, "Jet Effects on Coflow Jet Airfoil Performance," *AIAA Journal*, Coral Gables, FL, 2007.
- [10] A. Lefebvre, B. Dano, W. B. Bartow, M. D. Fronzo and G. Zha, "Performance and Energy Expenditure of Coflow Jet Airfoil with Variation of Mach Number," in *AIAA Paper 2013-0490*, *AIAA Journal of Aircraft*, 2016, pp. 1757-1767.
- [11] Y. Wang, Y. Yang and G. Zha, "Study of Super-Lift Coefficient of Co-Flow Jet Airfoil and Its Power Consumption," in *AIAA AVIATION Forum*, Dallas, TX, 2019.
- [12] Y. Yang and G. Zha, "Numerical Investigation of Performance Improvement of the Co-Flow Jet Electric Airplane," in *AIAA AVIATION Forum*, Atlanta, GA, 2018.
- [13] Y. Yang and G. Zha, "Super-Lift Coefficient of Active Flow Control Airfoil: What is the Limit?," in *AIAA SciTech Forum*, Grapevine, TX, 2017.
- [14] P. R. Spalart and S. R. Allmaras, "A One-Equation Turbulence Model for Aerodynamic Flows," in *30th Aerospace Sciences Meeting and Exhibit, Aerospace Sciences Meetings, AIAA 92-0439*, Reno, NV, USA, 1992.
- [15] Y. Shen and G. Zha, "Large Eddy Simulation Using a New Set of Sixth Order Schemes for Compressible Viscous Terms," in *Journal of Computational Physics, Vol. 229*, 2010, pp. 8296-8312.
- [16] G. Zha, Y. Shen and B. Wang, "An improved low diffusion E-CUSP upwind scheme," in *Journal of Computers and Fluids, Vol. 48*, 2010, pp. 214-220.

- [17] Y. Shen and G. Zha, "Generalized finite compact difference scheme for shock/complex flowfield interaction," in *Journal of Computational Physics*, Vol. 230, 2011, pp. 4419-4436.
- [18] Y. Shen, G. Zha and B. Wang, "Improvement of Stability and Accuracy for Weighted Essentially Nonoscillatory Scheme," in *AIAA Journal*, Vol. 47, 2009, pp. 331-344.
- [19] Y. Shen, G. Zha and X. Chen, "High Order Conservative Differencing for Viscous Terms and the Application to Vortex-Induced Vibration Flows," in *Journal of Computational Physics*, Vol. 228, 2009, pp. 8283-8300.
- [20] Y. Shen and G. Zha, "Improvement of the WENO scheme smoothness estimator," in *International Journal for Numerical Methods in Fluids*, 2010, pp. 653-675.
- [21] G. Zha and E. Bilgen, "Numerical Study of Three-Dimensional Flows Using Unfactored Upwind-Relaxation Sweeping Algorithm," in *Journal of Computational Physics*, Vol. 125, 1996, pp. 425-433.
- [22] B. Wang, B. Haddoukessouni, J. Levy and G. Zha, "Numerical Investigations of Injection Slot Size Effect on the Performance of Co-Flow Jet Airfoil," in *AIAA Journal of Aircraft*, Vol. 45, 2008, pp. 2084-2091.
- [23] Z. Liu and G. Zha, "Transonic Airfoil Performance Enhancement Using Co-Flow Jet Active Flow Control," in *AIAA Paper 2016-3472, AIAA Aviation*, 2016.
- [24] A. Lefebvre and G. Zha, "Trade Study of 3D Co-Flow Jet Wing for Cruise and Takeoff/Landing Performance," in *AIAA Paper 2016-0570, AIAA Aerospace Science Meeting*, San Diego, CA, USA, 2016.
- [25] B. Wang and G. Zha, "Detached-Eddy Simulation of a Coflow Jet Airfoil at High Angle of Attack," in *AIAA Paper 2009-4015, Journal of Aircraft*, 2011.
- [26] H.-S. Im, G. Zha and B. P. E. Dano, "Large eddy simulation of coflow jet airfoil at high angle of attack," in *Journal of Fluid Engineering*, Vol. 136(2), 2014.